JUSTIFICATION FOR HIGH VELOCITY IMPACT TESTING USING AS-BUILT AND STRESS RELIEVED DMLS TI6AL4V (ELI) BASED ON RESULTS FOR WROUGHT TI6AL4V

T.C. Moleko[1], M. Maringa[2] & W.B. duPreez[3]

[1, 2] Department of Mechanical and Mechatronics Engineering
[3]Centre for Rapid Prototyping and Manufacturing
Faculty of Engineering, Built Environment and Information Technology
Central University of Technology, Free State, Bloemfontein
South Africa

ABSTRACT

High velocity impact testing on wrought Ti6Al4V reported in an earlier paper, confirmed the potential of using this alloy for ballistic armour applications. Given the level of design freedom offered by additive manufacturing, complex armour applications could be produced through Direct Metal Laser Sintering of Ti6Al4V. Based on the test results obtained for wrought Ti6Al4V, this paper presents a justification for investigating the high velocity impact properties of as-built and stress relieved Direct Metal Laser Sintering Ti6Al4V (ELI). The calculations in this justification use the theories of the V_{50} ballistic limit and absorbed strain energy to estimate the optimum thickness of the material.

[1] The author is enrolled for a Master of Engineering degree in Mechanical Engineering in the Department of Mechanical and Mechatronics Engineering at the Central University of Technology Free State, South Africa.
*Corresponding author moleko_t@yahoo.com

1. INTRODUCTION

During the 1950s and 1960s aluminium alloy AA 5083 and also Rolled Homogeneous Armour steel (RHA) were developed for ballistic armour and have been widely used ever since [1][2]. In spite of the fact that RHA and AA 5083 are still traditionally used today, they do have some limitations in their respective applications [2].

The major disadvantages of AA 5083 are its low specific strength of 130 MPa-cm^3/kg and the low values of strength of its welded joints, which do not exceed 300 MPa [2]. RHA on the other hand, has a higher specific strength of 150 MPa-cm^3/kg, but this comes at the expense of significantly increased weight due to its high density of 7.8 g/cm^3 [2][3]. Plates of similar dimensions of the lower density wrought Ti6Al4V of 4.2 g/cm^3 give a weight saving of about 46% over RHA [2][3].

According to the military standard MIL-A-12560H (MR), it normally takes an 11.43 mm thick RHA plate to stop a 7.62 x 39 mm projectile also called a .30 calibre bullet travelling at about 700 m/s. Moreover, according to the military standard MIL-DTL-46027K (MR), it normally takes an AA 5083 plate with a thickness greather than 19.8 mm to stop the same projectile travelling at the same velocity.

To qualify an armour material prior to testing as having good ballistic performance, the material should have a high hardness so as to blunt projectiles and also high ductility to absorb the energy from projectiles during impact [1][2]. In the velocity range of about 700 m/s the performance of the wrought Ti6Al4V used for the preliminary testing does not fall too far short from that of RHA and is better than that of AA 5083; the two materials traditionally used this way [1], [2], [4]. In a previous paper, a 14 mm thick plate of wrought Ti6Al4V with a hardness of 300 BHN was observed to partially stop a 7.62 x 39 mm projectile moving at an average velocity of 701.18 m/s [4].

For manufacturing of complex parts from RHA and AA 5083 in the military industry welding is normally used to join parts together in order to achieve various desired shapes [3][5]. Welding joints are problematic because they act as stress concentration sites that can eventually bring about fatigue cracking of the manufactured parts [2]. Additive manufacturing has the advantage of being able to achieve complex geometries that are otherwise difficult, if not impossible, to produce using conventional methods of manufacturing without resorting to welding [6][7].

Additively manufactured Ti6Al4V (ELI) with its higher value of hardness (326 BHN) compared to the wrought alloy with a hardness of 300 BHN is expected to perform better by providing more effective blunting of the projectiles and hence achieving better resistance to penetration [8][9]. Furthermore, its higher value of yield strength (1089 MPa) compared to that of wrought Ti6Al4V (948 MPa) implies a higher capacity to absorb energy during plastic deformation and therefore a higher capacity to stop the penetration of projectiles [9][10].

This paper presents a justification for high velocity impact use of as-built and stress relieved direct metal laser sintering (DMLS) Ti6Al4V (ELI), with reference to test results of wrought Ti6Al4V. The justification uses theoretical modelling to develop expressions for the V_{50} ballistic limit and absorbed strain energy of elastic and plastic deformation to estimate the optimum thickness of the material. Furthermore, the justification also uses a comparison between the microstructure of wrought Ti6Al4V and as-built and stress relieved DMLS Ti6Al4V (ELI) to predict the performance of the latter under the same conditions.

In ballistics, new choices of materials such as ceramics, polymers, and polymer fibres and lower density metals have significantly decreased the weight of the armour needed for protection [2][12]. Although, ceramics continue to be studied they have a downside of low fracture toughness. Polymers suffer the setbacks of low impact strength and poor moisture resistance, which causes swelling of reinforcing fibres [11][12].

The failure of any single material to possess all required ballistic properties of high strength, hardness, stiffness and toughness, has led to the development of hybrid armour comprised of hard material at the front (the side facing the projectile) joined to ductile material at the back [2][12]. The hard material is used to blunt projectiles during impact, while the ductile material absorbs their energy [11]. Direct metal laser sintered Ti6Al4V is attractive because of its high specific values of strength, hardness and toughness, hence the reason for its study here.

2. THEORETICAL MODELING AND RESULTS

2.1 Justification Based on V_{50} Ballistic limit

The V_{50} ballistic limit or limit velocity (v_{bl}) is the velocity required for a projectile or impactor to reliably penetrate a particular piece of material without any residual velocity [11]. Furthermore, the penetration has to occur reliably at least 50% of the time [11][12].

An expression for the plastic work required to shear a plate and bring about failure by plugging can be developed from first principles. The expression is developed with an assumption that a plug pushed out of the plate has the same diameter as the projectile. By definition, work is done when a force that is applied to an object moves that object [13][14].

Based on this definition, the work done to bring about plugging of a target can thus be represented by the equation, $w_{Plug} = F \times x$, where the symbol w_{Plug} stands for the work done to bring about plugging, F the applied shear force and x the displacement of the plug being pushed out of the target. In the case of a suddenly applied load such as in ballistic impact, the foregoing equation can thus be expressed as an integral as shown in Equation (1) [14].

$$W_{Plug} = \int F \; dx \tag{1}$$

By definition a force is any interaction that when unopposed, will change the motion of an object [13][14]. In this case the applied shear force (F), is the force acting on a material in a direction parallel to the extension or deformation of the material and thus causing shearing of the target material to form a plug as shown in Figure 1. Figure 1 is a diagram illustrating plugging of a target material under ballistic impact.

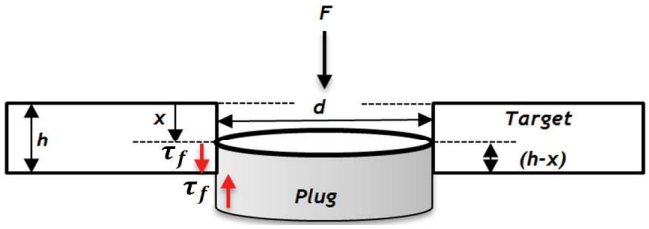

Figure 1: Plugging under ballistic impact

The projectile failure holes in the preliminary work on wrought Ti6Al4V were of the same transverse dimensions as the projectile. The projectile holes showed signs of friction around the middle which is thought to have been due to hole enlargement as the projectile forced its way through a leading narrower hole. The rugged edges of petalling signified rupture of fractured layers upon exit of the projectile. Clearly, the plug mode does not accurately represent penetration and failure for a projectile with a narrowed head. However, the method is quick and gives useful first estimates of the processes and therefore its adoption here.

From the failure shear stress (τ_f) and an elemental shearing area (dA), the elemental shear force (dF) can be represented by the equation $dF = \tau_f \times dA$, which when integrated gives a value of the total force necessary to push the plug out as $= \int \tau_f \times dA$.

The elemental shearing area (dA) is the area indicated in grey colour in Figure 1 and is represented by the equation $dA = \pi\, d\, (h - x)$, which when substituted into the expression for force generates the equation:

$$F = \int dF = \int \tau_f\, \pi\, d\, (h - x) \tag{2}$$

Substituting this equation into Equation (1) and introducing the integration limits yields:

$$W_{Plug} = \int_0^h \tau_f\ \pi\, d\, (h - x)\ dx \tag{3}$$

Noting that the shear failure stress is constant and taking this and other constant terms from inside the integral sign leads to:

$$W_{Plug} = \tau_f\, \pi\, d \left[\frac{h^2}{2}\right] = \frac{\tau_f\ \pi\ d\ h^2}{2} \tag{4}$$

Equation (4) can now be equated to the change in kinetic energy of the system to develop an expression for the ballistic limit (v_{bl}) and from it the optimum thickness (h_{opt}) required to resist through penetration [14]. The kinetic energy of the projectile is not all converted to work done during ballistic impact. The efficiency (η) of conversion of the kinetic energy to work of deformation is normally assumed to be constant and equal to 0.9 [15][16], thus:

$$\eta \Delta K_{kinetic} = W_{Plug} \tag{5}$$

$$\eta \left[\frac{1}{2} m_{proj} \left({v_{iproj}}^2 - {v_{fproj}}^2\right) - \frac{1}{2} m_{plug} \left({v_{iplug}}^2 - {v_{fplug}}^2\right)\right] = \frac{\tau_f\ \pi\ d\ h^2}{2} \tag{6}$$

In the foregoing expression the initial velocity of the plug $(v_{iplug} = 0)$, because the target is stationery before impact. Assuming also that the plug (v_{fplug}) and the projectile (v_{fproj}) have the same final velocity of $0\ m/s$ due to the fact that by definition of the ballistic limit the residual velocity should be so, Equation (6) then can be rewritten with the initial velocity of the projectile as the subject as follows:

$$v_{iproj} = \sqrt{\frac{\tau_f\ \pi\ d\ h^2}{0.9\ m_{proj}}} \tag{7}$$

In the ballistic impact tests done on wrought Ti6Al4V, an average initial velocity (v_{iproj}) of the projectile of 701.18 m/s was recorded for testing done for various thicknesses of wrought Ti6Al4V plates to investigate the optimum thickness [4].

At the optimum thickness of a target being impacted by a projectile travelling at a specific velocity, the initial velocity of the projectile and the ballistic limit are equal [12][14]. The optimum thickness can be calculated from the foregoing equation thus:

$$h_{opt} = \sqrt{\frac{0.9\ m_{proj}\ {v_{bl}}^2}{\tau_f\ \pi\ d}} \tag{8}$$

There are no published standard values for ultimate shear strength (τ_{max}) like with the ultimate tensile stress (σ_{uts}) and yield strength (σ_y). The shear strength can be calculated using the Tresca or Von Mises criterion which both yield a value of 0.5 for uniaxial loading [17][18]. This value ignores the effect of other principle stresses that develop during plastic shear failure under uniaxial loading and is therefore not adopted here [18].

The Taylor factor (M) and the ultimate tensile strength are used instead [19][20]. The Taylor factor is defined as the ratio of the sum of the magnitude of the slip system shear rate to the effective deformation rate [21]. The ultimate or failure shear strength can thus be calculated from the ratio of the Taylor factor and the ultimate tensile strength using the following equation [21].

$$\tau_{max} = \tau_f = \frac{\sigma_{uts}}{M} \tag{9}$$

In the case of ballistic impact tests conducted on wrought Ti6Al4V and future tests on DMLS Ti6Al4V (ELI) using a 7.62 x 39 mm projectile traveling at an average velocity of 701.18 m/s, an assumption is made that the increase of temperature during impact is significant enough to bring about an α (HCP) to β (BCC) transformation [4][24]. This assumption is made on the basis of findings that there is an adiabatic temperature rise that exceeds a 1000 K at an impact velocity of 550 m/s [24]. For BCC metals the appropriate Taylor factor (M) is 1.67 [25]. Table 1 below shows the mechanical properties of wrought and additively manufactured Ti6Al4V.

Table 1: Mechanical properties of wrought Ti6Al4V and DMLS Ti6Al4V (ELI)

Mechanical Property	Wrought Ti6Al4V (1)	DMLS Ti6Al4V (ELI) (2)
Elastic modulus (E) (Gpa)	105 [10]	112 [26]
Yield stress (σ_y) (MPa)	948 [10][27]	1098 [26]
Ultimate tensile stress (σ_{uts}) (MPa)	994 [10][27]	1265 [26]

From Table 1, the ultimate tensile strength of DMLS Ti6Al4V (ELI) and wrought Ti6Al4V are seen to be 1265 MPa and 994 MPa, respectively. Taking these values of ultimate tensile strength and the Taylor factor of 1.67 and then substituting them into Equation (9), to calculate the ultimate shear strength gives rise to:

DMLS Ti6Al4V

$$\tau_{max} = \tau_f = \frac{1265 \times 10^6}{1.67} = 757.5 \times 10^6\ Pa \tag{10}$$

Wrought Ti6Al4V

$$\tau_{max} = \tau_f = \frac{994 \times 10^6}{1.67} = 595.2 \times 10^6\ Pa \tag{11}$$

The projectile that was used for the preliminary testing on wrought Ti6Al4V is a 7.62 x 39 mm bullet, with a mass of 7.9 grams and a diameter of 7.9 mm [4]. Taking the known values of the parameters of the projectile and the values of ultimate shear strength calculated in Equations (10) and (11) and then substituting them into Equation (8) gives rise to:

DMLS Ti6Al4V

$$h_{opt} = \sqrt{\frac{0.9\ (7.9 \times 10^{-3})\ (701.18)^2}{(757.5 \times 10^6)\ \pi\ (7.9 \times 10^{-3})}} = 13.64\ mm \tag{12}$$

Wrought Ti6Al4V

$$h_{opt} = \sqrt{\frac{0.9\ (7.9 \times 10^{-3})\ \ (701.18)^2}{(595.2 \times 10^6)\ \ \pi\ \ (7.9 \times 10^{-3})}} = 15.38\ mm \tag{13}$$

From the tests done on wrought Ti6Al4V it was established that the optimum ballistic thickness of the alloy is greater than or equal to 14 mm [4]. Taking this into account a correction factor (CF) is determined from the calculated and the experimental values as follows:

$$CF = \frac{Calculated\ value - experimental\ value}{Calculated\ value} \times 100 \tag{14}$$

$$CF = \frac{15.38 - 14}{15.38} \times 100 \approx 9\ \% \tag{15}$$

Taking the correction factor for wrought Ti6Al4V calculated above and using it on DMLS Ti6Al4V to calculate the expected experimental value yields:

$$experimental\ value = Calculated\ value - \frac{CF\ \times Calculated\ value}{100} \tag{16}$$

$$experimental\ value = 13.64\ - \frac{9\ \times 13.64}{100} = 12.41\ mm \tag{17}$$

2.2 General Solution for the Absorbed Strain Energy in Cases of Gradually Applied Loads

Justification based on absorbed strain energy references the standard stress versus strain curve and considers the strain hardening phenomenon. Figure 2 shows the stress-strain curves of as-built SLM Ti6Al4V, annealed SLM Ti6Al4V and wrought Ti6Al4V.

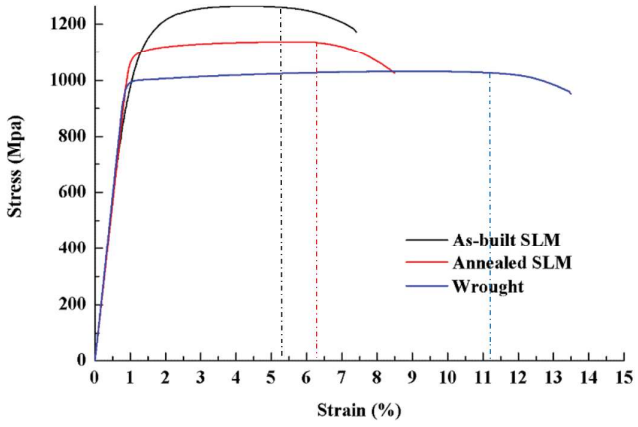

Figure 2: Stress-strain curves of As-built SLM Ti6Al4V, Annealed SLM Ti6Al4V and wrought Ti6Al4V [28].

From Figure 2 it can be seen that the non-uniform plastic deformation (from the advent of necking till fracture) part of the stress-strain curves makes up a very small percentage of the total deformation. Moreover, no equation was found in literature to describe this deformation. For this reason, the energy absorbed in this region is ignored in deriving the formula for estimation of the optimum ballistic thickness of DMLS Ti6Al4V (ELI).

Figure 3 is a stress-strain graph of two forms of DMLS Ti6Al4V (ELI) that exhibits no non-uniform plastic deformation. This further justifies ignoring the non-uniform plastic deformation shown in Figure 2.

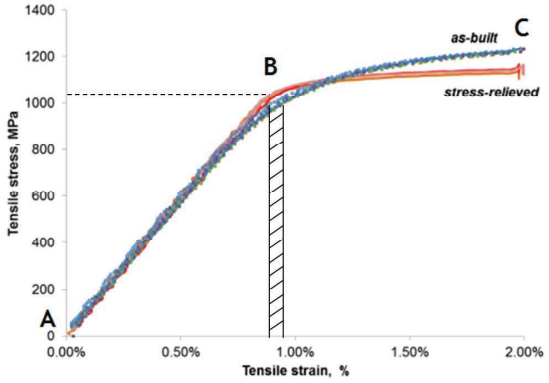

Figure 3: Stress-strain diagram of DMLS Ti6Al4V (ELI) [26].

Strain energy is defined as the energy stored in a body due to deformation as a result of work done on it [1][29]. During collision in ballistic impact, as the projectile makes contact with the target and deformation takes place the kinetic energy of the projectile is converted into strain energy in the target [1][29]. This therefore means that the loss in kinetic energy of the projectile is equal to the work done on the target, which is equal to the strain energy stored in the target [1][29]. There is an assumption in this that the projectile experiences minimal deformation and that negligible energy is absorbed through such deformation in it [2].

At failure and complete separation of a material, the total strain energy (U_T) stored in it is equal to the strain energy for elastic deformation (till the yield point indicated by point B in Figure 3), plus the strain energy for uniform plastic deformation that is characterised by strain hardening till ultimate fracture indicated by point C in the same figure.

For elastic deformation of a uniform target under a direct load the strain energy per unit volume (U_E) can be calculated using Equation (18) [30]. In these equations the symbol σ stands for the direct stress induced in the target, V the volume of the target and E the modulus of elasticity of the target.

$$U_E = \frac{{\sigma_y}^2}{2E} \times V = W_E \tag{18}$$

For the plastic region of deformation the strain energy per unit volume (U_P) can be calculated through an integration of the stress versus strain curve following two different approaches; one ere integration is carried out with reference to strain $(U_P = \int_{\sigma_y}^{\sigma_{uts}} \sigma\, V\, d\epsilon)$ and the other where integration is carried out with reference to stress $(U_P = \int_{\sigma_y}^{\sigma_{uts}} \sigma\, V\, d\epsilon)$, to yield the following equation:

$$U_P = V\left[\frac{K^{-\frac{1}{n}}}{n+1}\left[{\sigma_{uts}}^{\frac{n+1}{n}}\right] - \frac{K^{-\frac{1}{n}}}{n+1}\left[{\sigma_y}^{\frac{n+1}{n}}\right]\right] \tag{19}$$

But as stated earlier, the total strain energy stored in a material is equal to the sum of the elastic and plastic strain energies stored in the material, therefore:

$$U_T = U_E + U_P \tag{20}$$

$$U_T = \frac{{\sigma_y}^2}{2E} V + V\left[\frac{K^{\frac{1}{n}}}{n+1}\left[{\sigma_{uts}}^{\frac{n+1}{n}}\right] - \frac{K^{-\frac{1}{n}}}{n+1}\left[{\sigma_y}^{\frac{n+1}{n}}\right]\right] \quad (21)$$

2.3 Justification Based on Absorbed Strain Energy

The two approaches adopted for the strain energy stored in a material (U_T) are ideal for a case of gradual axial loading till fracture. However, in a case of transverse loading such as in ballistic impact, there is no opportunity for direct deformation because of the high strain rates prevailing and the target fails solely by shearing. In this case, the expression for shear strain energy per unit volume ($U_{E(\tau)}$) during elastic deformation of a uniform target under shear is applied and is expressed as follows.

$$U_{E(\tau)} = \frac{{\tau_y}^2}{2E} \times V = W_{E(\tau)} \quad (22)$$

In this equation the symbol τ_y stands for the shear yield stress of the material. The shear yield stress (τ_y) can be calculated from the direct stress using the Tresca or von Mises criterion, which both give the shear stress to be half the value of the direct stress elastic deformation [17], [18], [30].

The assumption is made here that there is no strain hardening during shear failure and that deformation beyond yield is purely plastic [31]. For the plastic region of deformation, the shear strain energy per unit volume ($U_{P(\tau)}$) is equal to the average work done to bring about plugging (W_{Plug}) which entails shear failure of the material [14]. The plastic shear strain energy per unit volume ($U_{P(\tau)}$) can thus be calculated using Equation (23) as:

$$U_{P(\tau)} = W_{Plug} = \frac{\tau_f \, \pi \, d \, h^2}{2} = \frac{\tau_y \, \pi \, d \, h^2}{2} \quad (23)$$

As established in the earlier calculations, the total strain energy stored in a material is equal to the sum of the elastic and plastic strain energies stored in the material. This is also the case for the total shear strain energy $(U_{T(\tau)})$ thus:

$$U_{T(\tau)} = U_{E(\tau)} + U_{P(\tau)} \quad (24)$$

$$U_{T(\tau)} = \frac{(\tau_y)^2}{2E} \times V + \frac{\tau_y \, \pi \, d \, h^2}{2} \quad (25)$$

From the tests done on wrought Ti6Al4V it was established that the optimum ballistic thickness of the alloy is greater than or equal to 14 mm [4]. Assuming the same amount of energy exerted by the projectile on the wrought Ti6Al4V and the DMLS Ti6Al4V (ELI), the total shear strain energies of the two can be equated to one another and the optimum ballistic thickness of DMLS Ti6Al4V (ELI) calculated. Such calculation assumes the same front area (A) for the two metals. Wrought Ti6Al4V is denoted with subscript 1 and DMLS Ti6Al4V (ELI) with subscript 2, to generate the following expression.

$$U_{T_1} = U_{T_2} \quad (26)$$

$$\frac{\left(\tau_{y_1}\right)^2}{2E_1} \times V_1 + \frac{\tau_{y_1} \, \pi \, d \, h_1^2}{2} = \frac{\left(\tau_{y_2}\right)^2}{2E_2} \times V_2 + \frac{\tau_{y_2} \, \pi \, d \, h_2^2}{2} \quad (27)$$

The shear yield strength of wrought Ti6Al4V and SLM Ti6Al4V (ELI) are 523 MPa and 634 MPa, respectively [32][33]. Furthermore, from Table 1 the elastic modulus (E) of wrought Ti6Al4V

and DMLS Ti6Al4V (ELI) are 105 GPa and 112 GPa, in that order. The projectile that was used for the preliminary testing on wrought Ti6Al4V is a 7.62 x 39 mm bullet, with a mass of 7.9 grams and a diameter of 7.9 mm [4].

Noting that areas (A_1) and (A_2) are equal, Equation (27) can be rewritten as:

$$\frac{\left(\tau_{y_1}\right)^2}{2E_1} \times h_1 + \frac{\tau_{y_1}\, \pi\ d\ h_1^2}{2} = \frac{\left(\tau_{y_2}\right)^2}{2E_2} \times h_2 + \frac{\tau_{y_2}\, \pi\ d\ h_2^2}{2} \tag{28}$$

Substituting in the known values of the parameters in Equation (28) gives rise to:

$$\frac{\left(523 \times 10^6\right)^2}{2(105 \times 10^9)} \times 0.014 + \frac{\left(523 \times 10^6\right)\ \pi\ \left(7.9 \times 10^{-3}\right)\ 0.014^2}{2} = \frac{\left(634 \times 10^6\right)^2}{2(112 \times 10^9)} \times h_2 + \frac{\left(634 \times 10^6\right)\ \pi\ \left(7.9 \times 10^{-3}\right)\ h_2^2}{2} \tag{29}$$

$$7.867 \times 10^6\, h_2^2 + 1.794 \times 10^6\, h_2 - 19.507 \times 10^3 = 0 \tag{30}$$

Equation (30) is a quadratic equation in terms of the parameter h, whose general solution is equal to;

$$h = \frac{-(1.794 \times 10^6) \pm \sqrt{(1.794 \times 10^6)^2 - 4(7.867 \times 10^6)(-19.507 \times 10^3)}}{2(7.867 \times 10^6)} \tag{31}$$

$$h = 10.399 \times 10^{-3} \quad and \quad h = -238.44 \times 10^{-3} \tag{32}$$

In Equation (50) the discriminant $(b^2 - 4ac) > 0$, therefore the quadratic equation has two real roots as seen in Equation (32). Based on the fact that the solution in this case is for a real dimension of a plate, the positive root is the logical choice between the two roots.

$$\therefore h = 10.399\ mm \approx 10.4\ mm \tag{33}$$

2.4 Justification Based on Microstructure

Comparison of the microstructures of as-built and stress relieved DMLS Ti6Al4V (ELI) and wrought Ti6Al4V provides further insight into the former as a better candidate than the latter for high velocity impact applications. At room temperature the microstructure at equilibrium of Ti6Al4V alloy consists mainly of the hexagonal close packed α phase with some retained body centered cubic β phase [22][23]. As the temperature is raised the alloy undergoes a α to β transformation [22][23]. The lowest temperature at which a 100% β phase can exist is called the beta transus and it is about 995°C [22]. Figures 4 and 5 show the microstructure of wrought Ti6Al4V and DMLS Ti6Al4V, respectively.

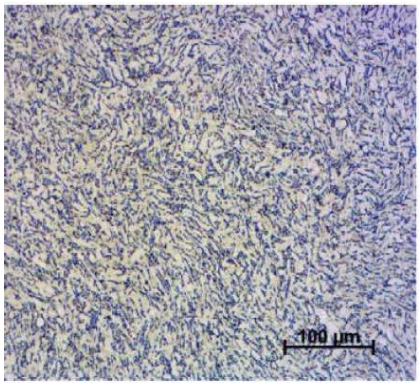

Figure 4: Microstructure of wrought Ti6Al4V [8]

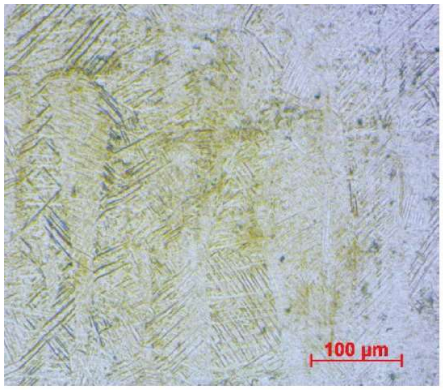

Figure 5: Microstructure of SLM Ti6Al4V [8].

Wrought Ti6Al4V has an equiaxed microstructure, while as-built and stress relieved SLM Ti6Al4V has a martensitic α' microstructure [8][26][37]. This fine microstructure avails more grain boundaries which in turn provide better resistance to crack propagation in the alloy over the wrought Ti6Al4V [26][37]. Additionally, the fine microstructure of the as-built and stress relieved SLM Ti6Al4V also has higher values of hardness, strength and stiffness over wrought Ti6Al4V [8]. The higher hardness comes with an advantage of having a better blunting effect of the projectile during impact, while the higher strength and stiffness offer more absorption of energy before failure of the target material [1][2].

3. RESULTS AND DISCUSSSION

Table 2 shows the calculated optimum thicknesses from each approach adopted here.

Table 2: Calculated values of optimum ballistic plate thicknesses

Material	Density (g/cm^3)	Description	Optimum thickness (mm)
Wrought Ti6Al4V	4.2	Calculated V_{50} ballistic limit	15.38
		Experimental ballistic limit	≥14 [4]
As-built and stress relieved DMLS Ti6Al4V (ELI)	4.2	Calculated V_{50} ballistic limit	13.64
		Corrected calculated V_{50} ballistic limit	12.41
		Calculated ballistic limit based on the absorbed shear strain energy	10.40
RHA	7.8	Military standard MIL-A-12560H (MR): Military specification for armour plate, steel, wrought, homogeneous (for use in combat-vehicles and for ammunition testing)	11.43
AA 5083	2.7	Military standard MIL-DTL-46027K (MR) Military specification for armour plate, aluminium alloy, weldable 5083, 5456 and 5059.	19.80

From Table 2 it can be seen that the calculated values of optimum thickness of as-built and stress relieved DMLS Ti6Al4V (ELI) of 13.41 mm and 10.40 mm respectively, based on the V_{50} ballistic limit and shear strain energy are lower than those of wrought Ti6Al4V of 15.38 mm and 14 mm, based on theoretical calculations of V_{50} ballistic limit and experimental results, respectively. The difference between the experimental and V_{50} ballistic limits for wrought

Ti6Al4V can be attributed to the fact that the non-uniform plastic and elastic deformation of the material was not considered in the calculations.

Taking this into consideration, the difference between the two was expressed as a correction factor of 9 % in Equation (29) and then applied to the calculated V_{50} ballistic limit obtained for as-built and stress relieved DMLS Ti6Al4V (ELI) to give a final value of expected experimental optimum thickness of 12.41 mm. In the calculations based on shear strain energy, the comparatively much lower value of 10.41 mm obtained can be attributed to the disregard of the non-uniform plastic deformation of the material; wrought and as built and stress relieved DMLS Ti6Al4V (ELI). While theory normally assumes pure plastic deformation after yield, the work of Somnath Chattopadhyay and Byoungchul Hwang shows this not to be entirely so, and small amounts of shear strain hardening do occur in practice [35][36]. The much lower value implies a larger shear strain hardening effect for the wrought alloy than the DMLS alloy, and therefore a larger error of calculation for the former than the latter, when ignoring this effect.

The optimum plate thickness of 10.40 mm calculated for as-built and stress relieved DMLS Ti6Al4V (ELI) using the strain energy approach is significantly lower than those of RHA and AA 5083 at 11.43 mm and 19.8 mm, respectively. The calculated V_{50} optimum plate thickness of 12.41 mm is marginally higher than the value for RHA and significantly lower than the value for AA 5083. Considering the effects of the densities of RHA, AA 5083 and Ti6Al4V of 7.8 g/cm^3, 2.7 g/cm^3 and 4.2 g/cm^3, in that order, the as-built and stress relieved DMLS Ti6Al4V (ELI) with a density of 4.2 g/cm^3 gives a weight saving of about 46% over RHA for plates of the same in-plane sizes.

The foregoing analysis shows that as-built and stress relieved DMLS Ti6Al4V (ELI) is expected to perform better under ballistic impact than the wrought Ti6Al4V. Therefore, ballistic testing with the DMLS Ti6Al4V (ELI) is recommended to validate the theoretically determined values and with anticipation that the material would yield better ballistic impact properties than wrought Ti6Al4V.

4. CONCLUSIONS

The deviation of the theoretical calculations from the experimental results of optimal thickness is 9 %. This deviation can be attributed to not considering the non-uniform plastic deformation of the material before failure, which is not the case in reality. In estimating the minimum plate thickness using the V_{50} ballistic limit, a correction factor of 9 % should be used to adjust the calculated value of thickness down.

It is safer to use the higher value of calculated minimum thickness of penetration for as-built and stress relieved DMLS Ti6Al4V of 12.41 mm obtained from the method of V_{50} ballistic limit, over the lower value of 10.40 mm obtained from the method of shear strain energy, as the former is the more conservative estimate.

The lower calculated values of minimum thickness for DMLS Ti6Al4V (ELI) imply expected better performance of the material in comparison to thicknesses of RHA steel of 11.43 mm, AA 5083 of 19.8 mm and wrought Ti6Al4V of 14 mm. This justifies further investigation into the high velocity impact performance of the additively manufactured alloy.

As the calculations done here are based solely on the strength and deformation of the impacted plate, considerations of hardness are expected to further decrease the optimum thickness it of DMLS Ti6Al4V as-built and stress relieved plates.

5. AKNOWLEDGEMENTS

The active support and funding of the South African Department of Science and Innovation through the CSIR for the Collaborative Program in Additive Manufacturing, Contract No.: CSIR-NLC-CPAM-18-MOA-CUT-01, are gratefully acknowledged.

REFERENCES

[1] **Lakshmana C. Rao, Narayana V. Murthy and Yogendra K. R. Simha**, 2016. *Applied impact mechanics*. 1st Edition. West Sussex: John Wiley & Sons Ltd.

[2] **Paul J. Hazell**, 2016. *Armour: Materials, Theory and Design*. 1st Edition. Canberra: CRC Press.

[3] **Cimpoeru S.J.,** 2016. The mechanical metallurgy of armour steels. *Technical Report*. Fishermans Bend: Austalian Land Division Defence Science and Technology Group.

[4] **Teboho C. Moleko, M. Maringa, W.B. du Preez,** Wrought Ti6Al4V as an alloy for high velocity impact applications, *Design and Additive Manufacturing of Titanium Parts pre-conference seminar, Proceedings of the 20th RAPDASA Annual International Conference, Emoya Estate, Bloemfontein, 5 - 8 November 2019*, pp. 66 – 77, ISBN 978-0-6398390-0-4.

[5] **Harry Bikas and George Chryssolouris**, 2015. Additive manufacturing methods and modeling approaches: a critical review. *International Journal of Additive Manufacturing Technology*, 1(1), pp. 389-405.

[6] **Christoph Leyens and Manfred Peters**, 2003. *Titanium and Titanium Alloys. Fundamentals and Applications*. 1st Edition. WILEY-VCH Verlag GmbH & Co. KGaA, Weinheim.

[7] **Ian Gibson,** 2015. *Additive Manufacturing Technologies:3D Printing, Rapid Prototyping, and Direct Digital Manufacturing*. 2nd ed. New York. Springer.

[8] **Manikandakumar Shunmugavel, Ashwin Polishetty and Moshe Goldberg**, 2017. A comparative study of mechanical properties and machinability of wrought and additive manufactured (selective laser melting) titanium alloy-Ti-6Al-4V. *Rapid Prototyping Journal*, pp. 1-12.

[9] **R. Boyer, E.W. Collings and G. Welsch**, 1994. Materials Properties Handbook. *Titanium Alloys*. ASM International.

[10] **Manikandakumar Shunmugavela, Ashwin Polishetty and Guy Littlefair**, 2015. Microstructure and mechanical properties of wrought and Additive manufactured Ti-6Al-4V cylindrical bars. *Procedia Technology*, Volume 20, pp. 231-236.

[11] **N. A. Rahman, S. Abdullah, W. F. H. Zamri and M. F. Abdullah.**, 2016. Ballistic Limit of High-Strength Steel and Al7075-T6 Multi-Layered Plates under 7.62-mm Armour Piercing Projectile Impact. *Latin American Journal of Solids and Structures*, pp. 1658-1676.

[12] **Tansel Deniz**, 2010. Ballisitic Penetration of Hardened Steel Plates. *Thesis submitted to Middle East Technical University*, pp. 1-113.

[13] **D. M. Fern´andez, M. F. Carusela and C. D. El Hasi**, 2010. Work-Energy theorem in rotational reference frames.*Reseachgate*, pp. 1-10.

[14] **Donald E. Carlucci and Sidney S. Jacobson**, 2014. *Ballistics Theory and Design of Guns and Ammunition*. 2nd ed. New York: CRC Press.

[15] **D. Macdougall,** 2000. Determination of the Plastic Work Converted to Heat Using Radiometry. *Experimental Mechanics*, (3), pp.298-306.

[16] **Guruswami Ravichandran, Ares J. Rosakis, Jon Hodowany and Phoebus Rosakis**, 2006. On the conversion of plastic work into heat during high strain deformation. *Shock Compression of Condensed Matter*, pp.557-562.

[17] **R. Lagioia and A. Panteghini**, 2015. On the existence of a unique class of yield and failure criteria comprising Tresca, von Mises, Drucker–Prager, Mohr–Coulomb, Galileo–Rankine, Matsuoka–Nakai and Lade–Duncan. *Mathematical, Physical and Engineering Sciences*, pp.1-21.

[18] **R. T. Qu, Z. J. Zhang, P. Zhang, Z. Q. Liu and Z. F. Zhang**, 2016. Generalized energy failure criterion. *Scientific reports*, pp.1-7.

[19] **C. H. C´aceresa and P. Luka´c**, 2008. Strain hardening behaviour and the Taylor factor of pure magnesium. *Philosophical Magazine*, 88(7), pp. 977-989.

[20] **Brian J. Hayes, Brian W. Martin and Brian Welk**, 2017. Predicting tensile properties of Ti-6Al-4V produced via directed energy deposition. *Acta Materialia*, pp.120-133.

[21] **Motoaki Morita and Osamu Umezawa**, 2011. Slip Deformation Analysis Based on Full Constraints Model for α-Titanium Alloy at Low Temperature. *Materials transactions*, 52(8), pp.1595-1602.

[22] Robert Pederson, 2002. Microstructure and Phase Transformation of Ti-6Al-4V. *Masters Thesis*. LULEA University of Technology, pp. 2-30.
[23] J. Sieniawski, W. Ziaja, K. Kubiak and M. Motyka, 2013. Microstructure and Mechanical Properties of High Strength Two-Phase Titanium Alloys. *Titanium Alloys - Advances in Properties Control*, pp. 70-80.
[24] X.W. Chen, G. Chen and F.J. Zhang, 2008. Deformation and Failure Modes of Soft Steel Projectiles Impacting Harder Steel Targets at Increasing Velocity. *Experimental Mechanics*, 48, pp.335–354.
[25] U.F. Kocks, 1970. The relation between polycrystal deformation and single-crystal deformation. *Met. Trans.*, pp. 1121.
[26] M.G. Moletsane, P. Krakhmalev, N. Kazantseva and I. Yadroitsev, 2016. Tensile properties and microstructure of Direct-Laser sintered TI6AL4V (ELI) alloy. *South African Journal of Industrial Engineering*, 27(3), pp.110-121.
[27] Amanda Sterling, 2015. Fatigue behaviour of Additively Manufactured Ti-6Al-4V. *Procedia Engineering*, pp. 576 – 589.
[28] Peng Zhang, Allen Naihui He and David Zhengwen Zhang, 2019. Evaluation of Low Cycle Fatigue Performance of Selective Laser Melted Titanium Alloy Ti–6Al–4V. *Metals*, pp.2-16.
[29] William J. Stronge, 2000. *Impact Mechanics*. 1st Edition. New York: Cambridge University Press.
[30] P. P. Benham, R. J. Crawford and C. G. Armstrong, 1996. *Mechanics of Engineering Materials*. 2nd ed. Essex: Longman.
[31] Somnath Chattopadhyay, Jerry Qu, Adres Nuri and Syed Ali Hasan, 2017. Torsion Tests to Study Plastic Deformation in Ductile Materials. *American Society for Engineering Education*, pp.1-18.
[32] Dylan Agius, Kyriakos I. Kourousis and Chris Wallbrink, 2018. A Review of the As-Built SLM Ti-6Al-4V Mechanical Properties towards Achieving Fatigue Resistant Designs. *Metals*, 75(8), pp.1-28.
[33] Danilo A. Renzo and Emanuele Sgambittera, 2018. Multiaxial fatigue behavior of additive manufactured Ti-6Al-4V under in-phase stresses. *Procedia Structural Integrity*, 18, pp.914–920.
[34] Manikandakumar Shunmugavel, Moshe Goldberg, Ashwin Polishetty and Guy Littlefair, 2017. Chip formation characteristics of selective laser melted Ti–6Al–4V. *Australian Journal of Mechanical Engineering*, pp.1-18.
[35] Somnath Chattopadhyay, Jerry Qu, Adres Nuri and Syed Ali Hasan, 2017. Torsion Tests to Study Plastic Deformation in Ductile Materials. *American Society for Engineering Education*, pp.1-18.
[36] Byoungchul Hwang, 2005. Dynamic deformation behavior of ultrafine-grained low-carbon steels fabricated by equal-channel angular pressing. *Metallurgical and Materials Transactions A*, 36A, pp.389-397.
[37] Zaneta Anna Mierzejewska, Radovan Hudák and Jarosław Sidun, 2019. Mechanical Properties and Microstructure of DMLS Ti6Al4V Alloy Dedicated to Biomedical Applications. *Materials*, pp.1-17.